Mid-infrared laser operation of (Er0.07La0.10Y0.83)2O3 sesquioxide ceramic

Stanislav Balabanov, Pavel Loiko, Liza Basyrova, Dmitry Permin, Denis Kosyanov, Timofey Evstropov, Sergey Filofeev, Alain Braud, Patrice Camy

Mid-infrared laser operation of $(Er_{0.07}La_{0.10}Y_{0.83})_2O_3$ sesquioxide ceramic

Stanislav Balabanov[1,*], Pavel Loiko[2], Liza Basyrova[2], Dmitry Permin[1,3], Denis Kosyanov[1,4], Timofey Evstropov[1], Sergey Filofeev[1], Alain Braud[2], and Patrice Camy[2]

[1] G.G. Devyatykh Institute of Chemistry of High-Purity Substances of the RAS, 49 Tropinin St., 603137 Nizhniy Novgorod, Russia
[2] Centre de Recherche sur les Ions, les Matériaux et la Photonique (CIMAP), UMR 6252 CEA-CNRS-ENSICAEN, Université de Caen Normandie, 6 Boulevard Maréchal Juin, 14050 Caen Cedex 4, France
[3] N.I. Lobachevsky National Research University, 23a Gagarin Ave., 603950 Nizhny Novgorod, Russia
[4] Far Eastern Federal University, 10 Ajax Bay, Russky Island, 690922 Vladivostok, Russia

*E-mail: Balabanov@ihps-nnov.ru

Received xxxxxx
Accepted for publication xxxxxx
Published xxxxxx

Abstract

A transparent sesquioxide ceramic $(Er_{0.07}La_{0.10}Y_{0.83})_2O_3$ was fabricated by vacuum sintering at 1780 °C for 3 h with lanthana acting as a sintering additive. It was of single-phase nature (sp. gr. $Ia\bar{3}$) with a close-packed microstructure (average grain size: 17 μm, pore content: 5 ppmv) and high transparency of 80% at 1.1 μm. The La^{3+} ions induced additional ihomogeneous broadening in the absorption and emission spectra of Er^{3+} ions. For the $^4I_{11/2} \rightarrow {}^4I_{13/2}$ transition, the stimulated-emission cross-section σ_{SE} was 1.06×10^{-20} cm^2 at 2719 nm and the luminescence lifetimes of the $^4I_{11/2}$ / $^4I_{13/2}$ states amounted to 2.73 / 5.91 ms, respectively. A $(Er_{0.07}La_{0.10}Y_{0.83})_2O_3$ ceramic laser generated 300 mW at 2840 nm with a slope efficiency of 27.7% and a laser threshold of only 17 mW.

Keywords: transparent ceramic, sesquioxides, erbium ions, mid-infrared, optical spectroscopy, laser

1. Introduction

Cubic yttrium sesquioxide (yttria) Y_2O_3 is a well-known host material for doping with trivalent rare-earth ions [1,2]. It possesses a bixbyite or C-type structure (bixbyite is a $(Fe,Mn)_2O_3$ mineral) with sp. gr. T^7_h - $Ia\bar{3}$. Yttria offers two substitutional rare-earth sites with symmetries C_2 (3/4 of ions) and C_{3i} (1/4 of ions) both with VI-fold oxygen coordination, however, electric dipole transitions are forbidden for ions entering the latter sites [1]. Like other cubic sesquioxides, Y_2O_3 offer strong crystal fields leading to large Stark splitting of multiplets of the dopant ions in C_2 sites which results in broadband emission properties. As a host matrix, Y_2O_3 benefits from high thermal conductivity (κ = 12.8 Wm^{-1}K^{-1} at room temperature [3]), good thermo-mechanical properties, broadband transparency (0.24 – 9 μm) and relatively low phonon energy (among oxide materials). The latter is essential for reducing the rates of multiphonon non-radiative relaxation from excited-states of rare-earth ions, e.g., for emission in the mid-infrared.

Cubic Y_2O_3 doped with erbium (Er^{3+}) ions is attractive for laser operation in the mid-infrared, at 2.8 μm, according to the $^4I_{11/2} \rightarrow {}^4I_{13/2}$ electronic transition [4,5]. 2.8 μm lasers are of practical importance for medical applications.

As the melting point of Y_2O_3 is extremely high (2425 °C), the growth of single-crystals constitutes a complicated task. As an alternative, the transparent ceramic technology has emerged to offer rare-earth-doped Y_2O_3 ceramic laser elements. In this way, the sintering temperature can be reduced down to about 1800 °C. Still, making yttria ceramic of sufficient quality and

size for practical applications requires the use of costly and low-productivity methods, such as a combination of hot pressing or free sintering followed by hot isostatic pressing (HIPing) [6-9].

Mid-infrared laser operation of Er:Y_2O_3 ceramics was reported [4,5,10,11]. Sanamyan *et al*. designed a diode-pumped 2 at.% Er:Y_2O_3 ceramic laser delivering 380 mW at 2.7 μm with a slope efficiency of 15% [4]. Ding *et al*. developed a diode-pumped 7 at.% Er:Y_2O_3 ceramic laser with a slab geometry generating 13.4 W at 2.84 μm at the expense of a low slope efficiency of 16% and low beam quality [5]. Recently, Mužík *et al*. studied heavily doped ceramic, 15 at.% Er:Y_2O_3, yielding 0.95 W at 2.73 μm with still a moderate slope efficiency of 17.4% [11].

Increasing the processability of fabrication of Er:Y_2O_3 ceramics can be achieved by introducing sintering additives. Heterovalent Zr^{4+} or Hf^{4+} ions are among the most commonly used sintering additive for yttria [12,13]. However, the photodarkening of such media makes it almost impossible to use them in lasers [14]. Lanthana (La_2O_3) is another efficient sintering additive [15]. The 10 mol% La:Y_2O_3 solid solution is consolidated into laser-quality ceramics only by free vacuum sintering (without subsequent HIPing), as demonstrated previously for $(Yb_xLa_{0.10}Y_{0.9-x})_2O_3$ ceramics [16-18].

In the present work, we extend this approach to Er^{3+}-doped Y_2O_3 ceramics. $(Er_{0.07}La_{0.10}Y_{0.83})_2O_3$ ceramics were fabricated by vacuum sintering and their structural, spectroscopic and laser properties were studied, for the first time, to the best of our knowledge.

2. Fabrication of ceramic

The nanopowders of $(Er_{0.07}La_{0.10}Y_{0.83})_2O_3$ were obtained by the self-propagating high-temperature synthesis (SHS) with the use of metal nitrates as oxidants and metal acetates as a fuel. The starting reagents were A_2O_3 (A = Y, La, Er) oxides (purity: 4N, Polirit, Russia), nitric acid HNO_3 (6N), and acetic acid CH_3COOH (4N, Khimreaktiv, Russia).

At the first stage, yttrium acetate and nitrates of yttrium, erbium, and lanthanum were obtained by dissolving oxides in the respective acids. The aliquots of these solutions were mixed to obtain a SHS precursor containing the desired ratio of metals and nitrate and acetate groups in a molar ratio of 1.6:1. The precursor was dried and placed in a quartz flask in a furnace preheated to 750 °C. After combustion, the powder was calcined in air at 900 °C for 5 h. The powder deagglomeration was carried out in a planetary ball mill (ball diameter: 10 mm) with a silicon nitride grinding elements. The milling medium was absolute isopropyl alcohol, and the total time was 20 h in the mode of 10 min milling / 10 min cooling. After drying, the powder was again annealed at 900 °C for 1 h in air to remove residual organic compounds. The powder was then compacted uniaxially in a steel mold into tablets (Ø15 mm, thiskness: 2 – 2.5 mm) at a pressure of 250 MPa. The green-body sintering was carried out in a furnace with an oil vacuum (at a pressure of no more than 10^{-2} Pa), a graphite heat insulation, and tungsten heaters at 1780 °C for 3 h. The heating was carried out at a rate of 10 °C/min up to 900 °C, then at 4 °C/min up to the sintering temerature, and the cooling was carried out in the switched off furnace mode. The ceramic was then annealed in air at 900 °C for 5 h to reduce oxygen vacancies and was mirror-polished with diamond pastes and slurries from 50 down to 0.5 μm. The final sample thickness was 1.2 mm. The polished ceramic disk is shown in figure 1. It is transparent and rose-colored due to the Er^{3+} doping.

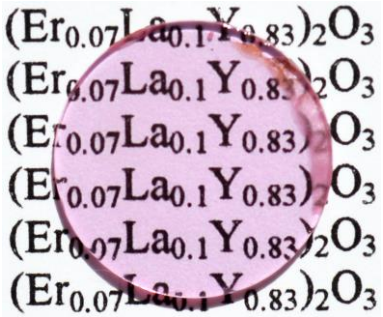

Figure 1. A photograph of an air-annealed and polished $(Er_{0.07}La_{0.10}Y_{0.83})_2O_3$ ceramic disk.

3. Results and discussion

3.1. Structural study

The typical morphology of sesquioxide powders obtained via SHS from acetatonitrate precursors is determined by nanosized primary particles combined into polydisperse agglomerates up to tens of μm in size [19,20]. The planetary ball milling allows to get rid of most of the agglomerates, however, some of them with a size about 1 μm and a rigid structure remain (figure 2). They are the most likely sources of pores in sesquioxide ceramics [21].

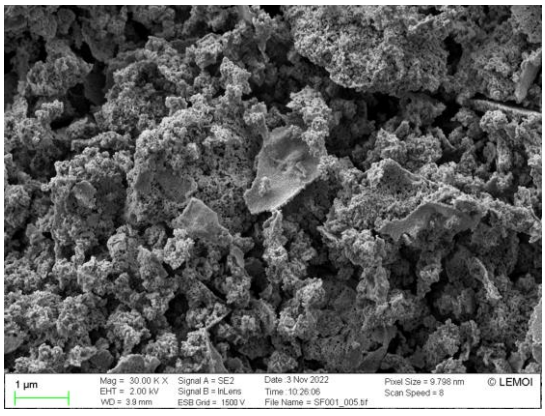

Figure 2. High-resolution scaning electron microscope (HRSEM) image of a planetary ball milled sesquioxide nanopowder $(Er_{0.07}La_{0.10}Y_{0.83})_2O_3$.

The specific surface area of the annealed $(Er_{0.07}La_{0.10}Y_{0.83})_2O_3$ powder was S_{BET} = 17.9±0.1 m^2/g, measured by the nitrogen adsorption according to the Brunauer–Emmett–Teller (BET) method.

As a rule, due to the mixing of components at the molecular level during the SHS synthesis of the precursor, solid-solution rare-earth sesquioxide powders are expected to be of single-phase nature. However, after sintering and / or subsequent annealing in air, in some cases, secondary phases enriched in lanthanum may be formed at the grain boundaries of ceramics [22]. The studied $(Er_{0.07}La_{0.10}Y_{0.83})_2O_3$ ceramic was of single-phase nature (cubic, bixbyite-type structure, sp. gr. $Ia\bar{3}$, lattice constant: a = 10.6664(3) Å, density: ρ_{calc} = 5.4011(4) g/cm^3), as confirmed by an X-ray powder diffraction (XRD) study, see figure 3. The relative intensities of diffraction peaks for the ceramic coincide with the theoretical ones for yttria (Y_2O_3), but their positions are shifted toward smaller angles due to the larger ionic radius of La^{3+} (1.032 Å) as compared to that of Y^{3+} (0.90 Å) and Er^{3+} (0.89 Å, for VI-fold oxygen coordination).

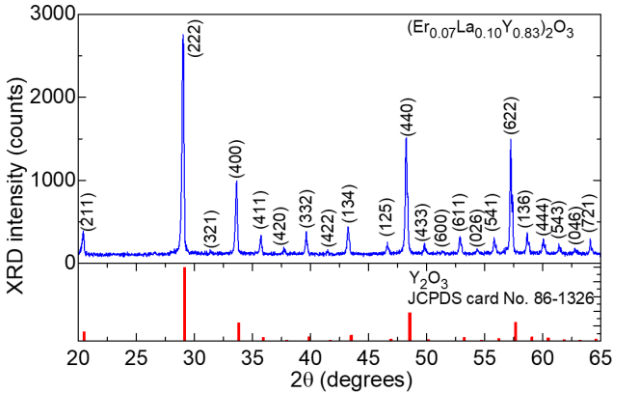

Figure 3. X-ray powder diffraction (XRD) pattern of the $(Er_{0.07}La_{0.10}Y_{0.83})_2O_3$ ceramic, *bars* – theoretical reflections for Y_2O_3 (JCPDS card No. 86-1326), *numbers* – Miller's indices (*hkl*).

A high-resolution scaning electrone microscope (HRSEM) image of a fracture surface of the ceramic, figure 4(a), reveals a close-packed microstructure and a lack of secondary phases at the grain boundaries. The average grain size is ~17 μm and the grain size distribution is relatively broad, as shown in figure 4(b). Intense grain growth in typical for La-doped yttria [23,24]. The growth of large grains (2-3 times the average size) can also be associated with the rigid agglomerates in the SHS powder. The removal of such agglomerates, e.g., by sedimentation is a prerequisite for further improving the optical quality of the ceramic.

In spite of the high grain growth rate during sintering, there is no pore-grain boundary separation with the formation of intragranular porosity. The residual sub-μm pores are located along the grain boundaries and in triple junctions and their clustering was not observed. This also leaves a room for improvement of the ceramic quality through a longer soaking time at the sintering temperature.

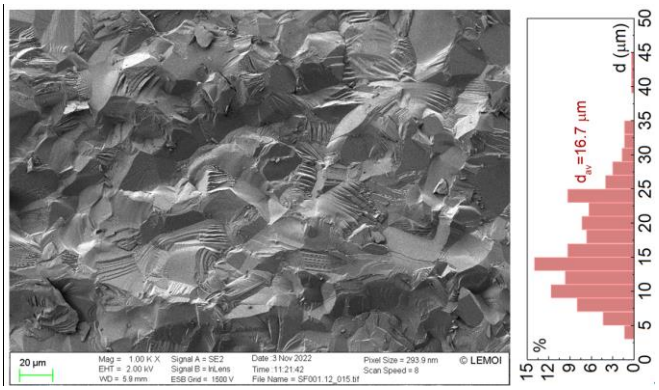

Figure 4. (a) HRSEM image of the fracture surface of the $(Er_{0.07}La_{0.10}Y_{0.83})_2O_3$ ceramic; (b) the corresponding grain size distribution.

A 3D visualization of the porous structure of the $(Er_{0.07}La_{0.10}Y_{0.83})_2O_3$ ceramic and a pore size distribution (according to the confocal laser scanning microscopy data) are shown in figure 5. An intuitive model proposed earlier was used to estimate the residual porosity of high-density materials as the fraction occupied by pores in the studied material volume [25]. The calculated residual porosity P is as small as 0.0005 vol% and the average pore size is 0.37 μm (with a maximum value of ~0.7 μm).

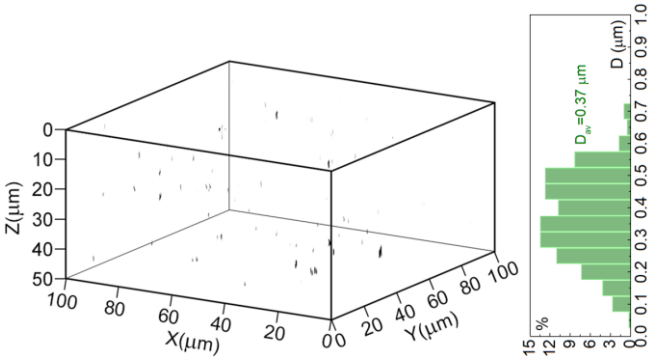

Figure 5. Analysis of porosity for the $(Er_{0.07}La_{0.10}Y_{0.83})_2O_3$ ceramic: (a) 3D confocal laser scanning microscopy observation of a volume of 100×100×50 $μm^3$; (b) pore size distribution.

3.2. Optical spectroscopy

Figure 6 shows the in-line transmission spectrum of an air-annealed and polished $(Er_{0.07}La_{0.10}Y_{0.83})_2O_3$ ceramic disk with a thickness of 1.2 mm. The ceramic exhibited a very broad transparency range, 0.24 – 9.5 μm. At ~1.1 μm, the ceramic disk had a high transmission of 80.0±0.5% being close to the theoretical limit set by Fresnel losses, $T_0 = 2n/(n^2 + 1)$ = 82.4% (accounting for multiple reflections, calculated based on the refractive index n = 1.900 [26]). A rather sharp rise of transmission near the UV transparency edge confirms the confocal microscopy data about the low

ceramic porosity, while the gradual rise of transmission with the wavelength supports our conclusion about the sub-μm and polydisperse structure of pores. The obtained data suggest that the pores are the main source of optical losses in the ceramic.

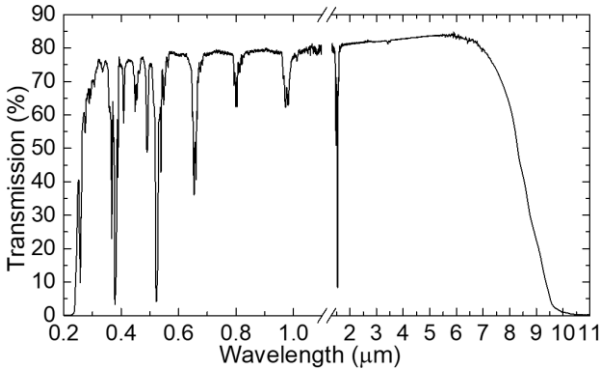

Figure 6. A transmission spectrum of an air-annealed and polished $(Er_{0.07}La_{0.10}Y_{0.83})_2O_3$ ceramic disk (thickness: t = 1.2 mm).

The Raman spectrum of the $(Er_{0.07}La_{0.10}Y_{0.83})_2O_3$ ceramic, figure 7(a), is typical for cubic bixbuite-type sesquioxides. The most intense peak appears at 370 cm^{-1} (the A_g + F_g modes [27]), and it is broadened and red-shifted with respect to that for a $(Er_{0.07}Y_{0.93})_2O_3$ ceramic (377 cm^{-1}) indicating a formation of a substitutional solid-solution.

The absorption cross-sections, σ_{abs}, for the $^4I_{15/2} \rightarrow {}^4I_{11/2}$ transition are shown in figure 7(b). They were calculated for an Er^{3+} concentration N_{Er} of 17.22×10^{20} at/cm^3. The peak σ_{abs} is 0.34×10^{-20} cm^2 at 981.3 nm and the corresponding absorption bandwidth (FWHM) is less than 1 nm and another broader peak is found at 971.1 nm (σ_{abs} = 0.22×10^{-20} cm^2). The absoprtion spectrum is less structured as compared to that for the $(Er_{0.07}Y_{0.93})_2O_3$ ceramic due to the La^{3+} codoping inducing additional inhomogeneous spectral broadening similarly to other "mixed" sesquioxde ceramics [28].

The stimulated-emission (SE) cross-sections, σ_{SE}, the $^4I_{11/2} \rightarrow {}^4I_{13/2}$ transition falling in to the mid-infrared spectral range were calculated using the Füchtbauer-Ladenburg formula [29]. The radiative lifetime of the emitting state (τ_{rad} = 5.39 ms) and the luminescence branching ratio ($B_{JJ'}$ = 18.3%) for Er^{3+} ions in yttria were calculated using the standard Judd-Ofelt theory. The mid-infrared emission spectra of Er^{3+} ions are very broad spanning from 2.6 to 3 μm and the maximum σ_{SE} is 1.06×10^{-20} cm^2 at 2719 nm, see figure 7(c). Due to the reabsorption from the metastable terminal laser level ($^4I_{13/2}$) caused by a resonant excited-state absorption, $^4I_{13/2} \rightarrow {}^4I_{13/2}$, the laser operation in Er^{3+} ions frequently occurs at longer wavelengths. For the studied ceramic, it is expected around 2849 nm (σ_{SE} amounts to 0.45×10^{-20} cm^2).

The luminescence decay curves from the upper ($^4I_{11/2}$) and lower ($^4I_{13/2}$) laser levels of Er^{3+} in the $(Er_{0.07}La_{0.10}Y_{0.83})_2O_3$ ceramic were measured under resonant excitation, as shown in figure 7(d). The mean luminescence lifetimes $<\tau_{lum}>$ are 2.73 ms and 5.91 ms, respectively, representing a favorable ratio for mid-infrared laser operation. For comparison, we also determined the corresponding luminescence lifetimes for an $(Er_{0.07}Y_{0.93})_2O_3$ ceramic, $<\tau_{lum}>$ = 2.74 ms and 5.88 ms, respectively, indicating a minor effect of La^{3+}.

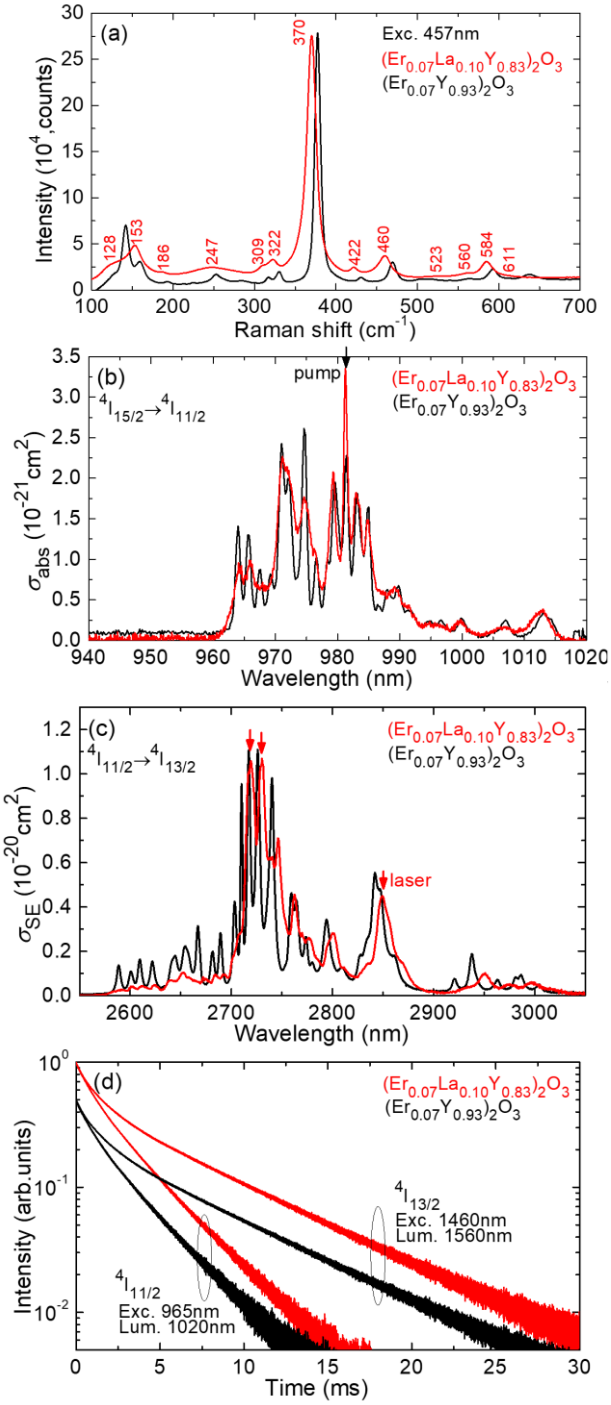

Figure 7. Spectroscopy of $(Er_{0.07}La_{0.10}Y_{0.83})_2O_3$ ceramic: (a) Raman spectrum, λ_{exc} = 457 nm; (b) absorption cross-sections, σ_{abs}, the $^4I_{15/2} \rightarrow {}^4I_{11/2}$ transition; (c) stimulated-emission (SE) cross-sections, σ_{SE}, the $^4I_{11/2} \rightarrow {}^4I_{13/2}$ transition; (d) luminescence decay curves from the $^4I_{11/2}$ and $^4I_{13/2}$ Er^{3+} states under resonant excitation. The data for a $(Er_{0.07}Y_{0.93})_2O_3$ ceramic are added for comparison.

3.3. Mid-infrared laser operation

The $(Er_{0.07}La_{0.10}Y_{0.83})_2O_3$ ceramic (Ø12 mm, t = 0.93 mm) was polished from both sides to laser-grade quality and left uncoated. It was mounted on a passively cooled Cu-holder using a silver paste for better heat removal. A simple linear hemispherical laser cavity was used. It was formed by a flat pump mirror (PM) coated for high transmission (HT) at 0.92 – 1.06 μm and high reflection (HR) at 2.6 – 3.0 μm, and a set of concave output couplers (OCs) having a radius of curvature (RoC) of -100 mm and a transmission at the laser wavelength T_{OC} in the range of 0.33% - 4.0%. The ceramic element was placed close to the PM with an airgap less than 1 mm. The total cavity length was about 100 mm.

As a pump source, we employed a continuous-wave Ti:sapphire laser (3900S, Spectra Physics) delivering up to 3.2 W at 981 nm with a diffraction-limited beam quality ($M^2 \approx 1$). The pumping was into the $^4I_{15/2} \rightarrow {}^4I_{11/2}$ absorption band of Er^{3+} ions. The pump beam was focused into the ceramic element through the PM using an AR-coated achromatic lens (focal length: f = 75 mm) resulting in a pump spot radius w_P of 33±5 μm (at the $1/e^2$ level). The measured single-pass pump absorption was 36.7%. The residual pump power was filtered out using a long-pass filter (LP1400, Spectrogon). The laser spectra were measured using an optical spectrum analyzer (AQ6376, Yokogawa).

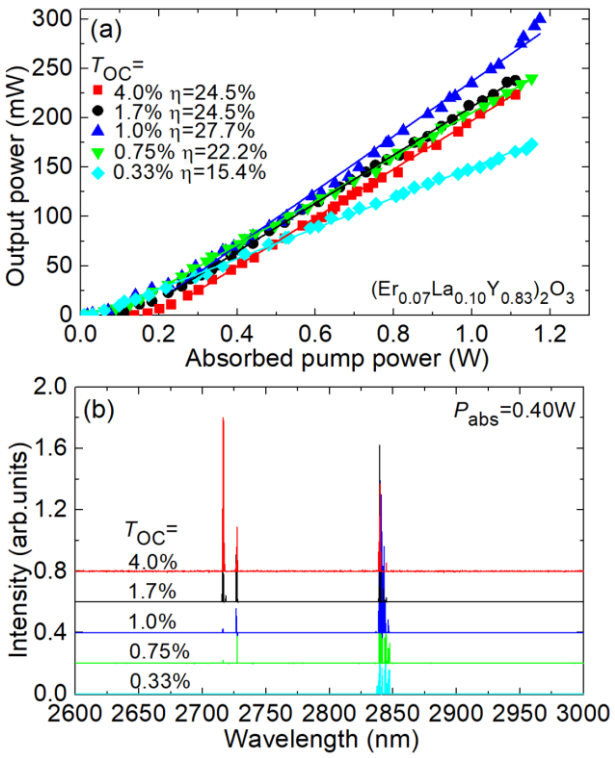

Figure 8. Mid-infrared $(Er_{0.07}La_{0.10}Y_{0.83})_2O_3$ ceramic laser: (a) input-output dependences, η – slope efficiency; (b) typical spectra of laser emission.

The mid-infrared $(Er_{0.07}La_{0.10}Y_{0.83})_2O_3$ ceramic laser generated a maximum output power of 300 mW at ~2840 nm with a slope efficiency η of 27.7% (with respect to the absorbed pump power) and a laser threshold of only 17 mW (for T_{OC} = 1.0%), figure 8(a). The laser threshold gradually increased with output coupling, from 9 mW (T_{OC} = 0.33%) to 135 mW (T_{OC} = 4%). The input-output dependences were linear well above the laser threshold. Further power scaling was limited by the relatively low pump absorption in a thin ceramic sample and the available pump power. It is expected by applying commercially available InGaAs laser diodes emitting at ~980 nm as pump sources.

The typical spectra of laser emission are shown in figure 8(b). For small output coupling ($T_{OC} \leq 1\%$), the laser operated at ~2840 nm and for higher T_{OC}, the laser emission was observed both at ~2716 and 2840 nm. The ceramic laser operated on the fundamental transverse mode (TEM_{00}).

4. Conclusions

To conclude, vacuum sintering at 1780 °C using sesquioxide nanopowders of complex composition $(Er,La,Y)_2O_3$ obtained via self-propagating high-temperature synthesis with La_2O_3 acting as a sintering additive is a viable and technologically simple way of fabricating highly transparent laser ceramics with a close-packed microstructure and a reasonably low content of pores. An $(Er_{0.07}La_{0.10}Y_{0.83})_2O_3$ ceramic fabricated in this way exhibits broadband mid-infrared emission owing to the $^4I_{11/2} \rightarrow {}^4I_{13/2}$ transition, an appealing ratio of the upper laser level ($^4I_{11/2}$) to lower laser level ($^4I_{13/2}$) luminescence lifetimes and enables efficient laser operation at 2.8 μm. The La^{3+} ions induce additional inhomogeneous broadening to the absorption / emission spectra of Er^{3+} ions. Further power scaling is expected by applying ~980 nm InGaAs laser diodes as pump sources.

Acknowledgements

This work was supported by the Russian Science Foundation (RSF) [21-13-00397] https://rscf.ru/en/project/21-13-00397/ and by the Normandy Region, France ("RELANCE" Chair of Excellence project).

References

[1] Kränkel C 2015 *IEEE J. Sel. Top. Quantum Electron*. **21** 250-62
[2] Fornasiero L, Mix E, Peters V, Petermann K and Huber G 2000 *Ceram. Int.* **26** 589-92
[3] Balabanov S, Evstropov T, Permin D, Postnikova O, Praded A and Popov P 2022 *Inorganics* **10** 78
[4] Sanamyan T, Simmons J and Dubinskii M 2010 *Laser Phys. Lett.* **7** 206–9
[5] Ding M, Li X, Wang F, Shen D, Wang J, Tang D and Zhu H 2022 *Appl. Phys. Express* **5** 062004.
[6] Balabanov S, Permin D, Evstropov T, Andreev P, Basyrova L, Camy P, Baranov M, Mateos X and Loiko P 2021 *Opt. Mater.* **119** 111349
[7] Wang Z, Zhang L, Yang H, Zhang J, Wang L and Zhang Q 2016 *Ceram. Int.* **42** 4238–45
[8] Yin D, Wang J, Liu P, Zhu H, Yao B, Dong Z and Tang D 2019

J. Am. Ceram. Soc. **102** 7462–8
[9] Xue Y, Zhu F, Wang J, Sun S, Hu L and Tang D 2021 *J. Rare Earths* **40** 1913–9
[10] Wang L, Huang H, Shen D, Zhang J, Chen H and Tang D 2017 *Opt. Mater.* **71**, 70–3
[11] Mužík J, Yasuhara R, Smrž M, Kubeček V and Mocek T 2019 *Laser Phys. Lett.* **16** 035801
[12] Osipov V V, Shitov V A, Maksimov R N and Solomonov V I 2015 *Opt. Mater.* **50** 65–70
[13] Yavetskiy R P, Balabanov A E, Parkhomenko S V, Kryzhanovska O S, Doroshenko A G, Mateychenko P V, Tolmachev A V, Li J, Jiang N, Gheorghe L and Enculescu M 2021 *J. Adv. Ceram.* **10** 49–61
[14] Wang J, Yin D, Ma J, Liu P, Wang Y, Dong Z, Kong L B and Tang D 2019 *J. Eur. Ceram. Soc.* **39** 635–40
[15] Rhodes W H, Wei G C and Trickett E A 1986 *Proc. SPIE* **683** 12–8
[16] Li S, Zhu X, Li J, Yavetskiy R, Ivanov M, Liu B, Liu W and Pan Y 2017 *Opt. Mater.* **71** 56–61
[17] Yang Q H, Ding J, Zhang H W and Xu J 2007 *Opt. Commun.* **273** 238–41
[18] Balabanov S S, Bykov Y V, Egorov S V, Eremeev A G, Gavrishchuk E M, Khazanov E A, Mukhin I B, Palashov O V, Permin D A and Zelenogorskii V V 2013 *Quantum Electron.* **43** 396–400
[19] Permin D A, Novikova A V, Gavrishchuk E M, Balabanov S S and Sorokin A A 2017 *Inorg. Mater.* **53** 1330–5
[20] Balabanov S S, Bykov Y V, Egorov S V, Eremeev A G, Gavrishchuk E M, Khazanov E A, Mukhin I B, Palashov O V, Permin D A and Zelenogorsky V V 2013 *Opt. Mater.* **35** 727–30
[21] Balabanov S, Filofeev S, Ivanov M, Kaigorodov A, Krugovykh A, Kuznetsov D, Permin D, Popov P and Rostokina E 2020 *Opt. Mater.* **101** 109732
[22] Balabanov S, Demidova K, Filofeev S, Ivanov M, Kuznetsov D, Li J, Permin D and Rostokina E 2020 *Phys. Status Solidi B* **257** 1900500
[23] Zhang L, Yang J, Yu H and Pan W 2020 *J. Adv. Ceram.* **9** 493–502
[24] Ivanov M, Kopylov Y, Kravchenko V, Li J, Medvedev A and Pan Y 2014 *J. Rare Earths* **32** 254–8
[25] Kosyanov D Y, Zavjalov A P, Vornovskikh A A, Zakharenko A M, Liu X and Li J 2021 *Ceram. Int.* **47** 28932–41
[26] Nigara Y 1968 *Jpn. J. Appl. Phys.* **7** 404–8
[27] Todorov N D, Abrashev M V, Marinova V, Kadiyski M, Dimowa L and Faulques E 2013 *Phys. Rev. B* **87** 104301
[28] Basyrova L, Loiko P, Jing W, Wang Y, Huang H, Dunina E, Kornienko A, Fomicheva L, Viana B, Griebner U, Petrov V, Aguiló M, Díaz M, Mateos X and Camy P 2021 *J. Lumin.* **240** 118373
[29] Aull B, Jenssen H 1982 *IEEE J. Quantum Electron.* **18** 925–30